# Fabrication of Ordered Catalytically Active Nanoparticles Derived from Block Copolymer Micelle Templates for Controllable Synthesis of Single-Walled Carbon Nanotubes

**Jennifer Lu,*,†,‡ Sung Soo Yi,† Thomas Kopley,† Cheng Qian,§ Jie Liu,§ and Erdogan Gulari‡**

*Agilent Laboratories, 3500 Deer Creek Road, Palo Alto, California 94304, Macromolecular Science & Engineering Program, University of Michigan, Ann Arbor, Michigan 48109-1055, and Department of Chemistry, Duke University, Durham, North Carolina 27708*

*Received: December 6, 2005; In Final Form: January 20, 2006*

We report the use of the block copolymer micelle approach to produce various transition metal nanoparticles such as iron, cobalt, and nickel with precisely controlled size and spacing. These uniformly sized catalyst nanoparticles derived from the block copolymer micelle approach have enabled the synthesis of carbon nanotubes (CNTs) with narrow size distribution. Because of the excellent film forming ability of the polymeric material, metal-bearing surface micelles produced from the solution micelles can be distributed uniformly on a surface, resulting in evenly dispersed catalyst nanoparticles. As a result, high quality and uniformly distributed CNTs have been synthesized. Spatially selective growth of CNTs from a lithographically patterned metal-bearing micelle film has been achieved. The polymer template approach can potentially be extended to synthesize single-metallic and bimetallic catalytically active nanoparticles with uniform size and spacing and is fully compatible with conventional lithographic process. Additionally, catalyst nanoparticles produced from this method do not coalesce at high growth temperature. All these attributes make this approach a promising fabrication pathway for controllable synthesis of CNTs.

## Introduction

There is great interest in both academia and industry in carbon nanotubes (CNTs) due to their unique electrical, thermal, and mechanical properties. Much research has been devoted to develop devices that utilize these novel attributes. For example, CNTs are being exploited as field-emitter tips in displays,[1] as transistors,[2] as interconnect and memory elements in integrated circuits,[3] as scan tips for atomic force microscopy,[4] and as sensor elements for chemical and biological sensing.[5] The major obstacle to commercialize CNT-based devices is the lack of a manufacturable synthesis method to produce CNTs with controllable and predictable diameter and density at predefined locations. Chemical vapor deposition has gained popularity for CNT growth in which CNTs are grown selectively on catalytic sites. Therefore the diameter, location, and density of CNTs are thus largely dependent on the size, placement, and interparticle distance of catalyst nanoparticles.[6] To achieve controllable synthesis of CNTs, it is essential to develop a catalyst preparation method which is capable of rationally controlling size, spacing, and location of catalytically active nanoparticles. It is well known that the diameter of catalyst nanoparticles needs to be less than 3 nm in order to produce single-walled CNTs. Such small diameter metallic nanoparticles cannot be produced easily by top-down lithography techniques, although some progress toward this goal has been made.[7] Conversely, bottom-up self-assembly techniques naturally produce nanoparticles of such small size.

Self-assembly techniques have been demonstrated as a powerful method to generate well-ordered structures on the nanometer scale. Block copolymers, a class of self-assembling macromolecules, can be spontaneously self-organized into well-defined spherical, cylindrical, and lamellar morphologies, which is dictated by the composition and volume ratio of the block copolymer. Over the last several years, fabricating nanostructures from self-assembled block copolymer templates has been actively pursued.[8−10] One of the applications is to employ block copolymers as nanoreactors to generate inorganic nanoparticles. In this approach, a block copolymer forms micelles in a solution where the solvent-unfavorable block forms the core and the solvent-favorable block comprises the corona. By introducing metallic species that selectively react with a functional group in the repeat unit of the solvent-unfavorable block, micelles with metal-bearing cores can be produced. By depositing a monolayer of these metal-loaded micelles onto a surface, metallic nanoparticles with controlled size and spacing can thus be produced after removal of the organic components and subsequent reduction. It has already been demonstrated that gold nanoparticles can be produced by this method and the size and spacing can be tailored by adjusting the chain lengths and the amount of gold loading. The typical size of the gold nanoparticles is less than 10 nm and can be as small as 1 nm.[11]

Iron nanoparticles prepared from self-assembled solution micelles have been successfully used as catalysts to grow CNTs.[12] However, neither the size nor the periodicity has been well controlled. In addition, catalyst nanoparticles other than iron prepared from the block copolymer micelle approach have not been explored for CNT growth. In this paper, we report using block copolymer solution micelle templates to produce a variety of transition metal nanoparticles such as iron, cobalt, and nickel with controlled size and periodicity. The uniformly sized catalytically active nanoparticles produced from this method have enabled the synthesis of CNTs with a narrow size distribution. Due to the excellent film forming ability of a

* To whom correspondence should be addressed. E-mail: Jennifer_lu@agilent.com.
† Agilent Laboratories.
‡ University of Michigan.
§ Duke University.

10.1021/jp057085g CCC: $33.50 
Published on Web 03/09/2006

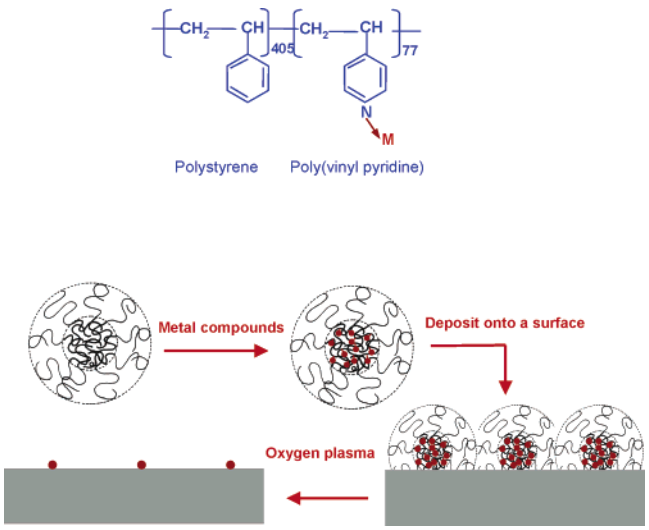


**Figure 1.** Schematic drawing of the formation of nanoparticles using the block copolymer micelle approach.

polymeric material, metal-containing micelles can be uniformly distributed across a wafer. Consequently, uniformly distributed catalyst nanoparticles can be produced, resulting in high quality and uniform density CNTs. Spatially selective growth of CNTs has been achieved by using top-down conventional lithography to pattern a metal-loaded micelle film. More significantly, the nanoparticles produced by this method do not agglomerate at the CNT growth temperature. The ability of the block copolymer micelle approach to produce uniformly sized and spaced nanoparticles which do not aggregate at the high growth temperature provides a promising pathway for diameter-controlled CNT synthesis.

## Experimental Section

**IR Study of Metal Complexation.** For this study, poly(4-vinyl pyridine) (denoted P4VP) homopolymer, purchased from Polymer Source, was dissolved in ethanol. Hydrated iron(II), cobalt(II), and nickel(II) chloride salts from Aldrich were then added with the amounts of the metal precursors adjusted to have a molar ratio of metal to pyridine of 0.25. The metal-containing solutions were then spotted on NaCl windows, and the solvent was removed in a vacuum at 80 °C. FTIR spectra were acquired using a Nicolet MagNA-IR 850.

**Nanoparticles.** Polystyrene-*b*-poly(4-vinyl pyridine) (denoted PS-b-P4VP hereafter) with a polystyrene $M_w$ of 42000 and poly-(4-vinyl pyridine) $M_w$ of 8100 was used as received from Polymer Source. The PS-b-P4VP block copolymer was first dissolved in toluene to form a 0.15 wt % solution. Hydrated iron(II), cobalt(II), and nickel(II) chloride salts were then stirred into the polymer solutions, and the amount of metal salts added was adjusted to obtain a molar ratio of metal to pyridine of 0.25. Spin-coating was used to deposit metal-bearing solution micelles onto 5000 Å coated silicon thermal oxide surfaces. UV-ozonation was used to remove all the organic components and leave the nonvolatile inorganic metal-containing nanoparticles behind. A DI-500 Digital Instrument atomic force microscope was used to analyze the height and distribution of nanoparticles. A Quantum 2000 X-ray photoemission spectrometer with an aluminum source was used to determine the chemical composition of as-synthesized nanoparticles.

**CNT Growth.** After thermolysis of various metal oxide nanoparticles at 700 °C in air, the substrates were heated to 900 °C under $H_2$. Under this reducing atmosphere, metal oxide

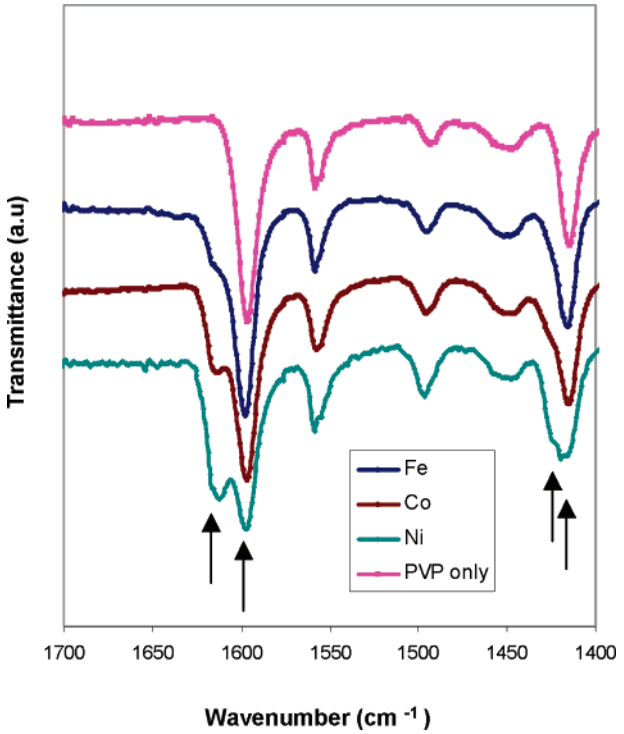


**Figure 2.** FTIR spectra of P4VP and metal-complexed P4VP.

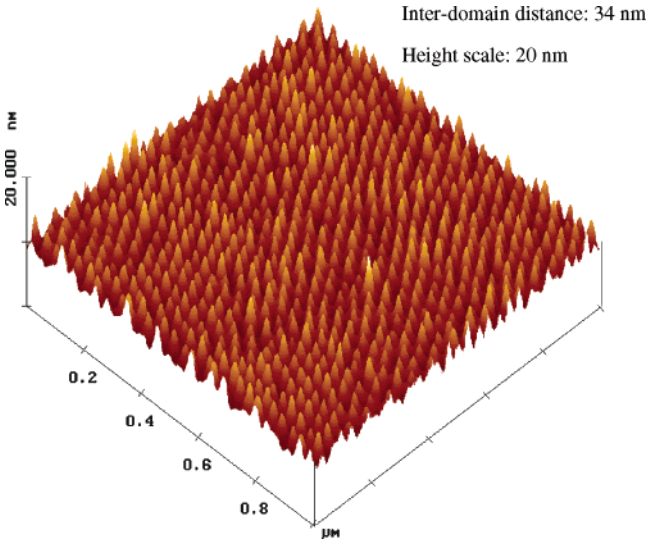


**Figure 3.** Three-dimensional AFM height image of surface micelles of PS-P4VP (1 $\mu$m by 1 $\mu$m).

nanoparticles were reduced to their zero valent metallic state. Subsequently either a mixture of methane and ethylene or methane alone was added to the gas flow to initiate carbon nanotube growth. After the growth, the carbon feed gases were switched off and the furnace was then cooled to room temperature under a flow of $H_2$ gas. CNTs were characterized by a Hitachi S-4500 SEM and the DI AFM. Raman spectroscopy was performed at Charles Evans Analytical Group in Sunnyvale, CA. For patterned carbon nanotube growth, a bilayer lift-off process was used to generate a patterned cobalt-bearing micelle film. Shipley LOL1000 was spun onto a 500 nm thermal oxide surface and then baked at 180 °C for 10 min to give a film with thickness of 100 nm. Subsequently an 800 nm thick OCG 825 resist film was formed on top of the LOL1000 layer by spin-coating and then baked at 105 °C for 3 min. This bilayer system was exposed using an ASML2500/40 stepper with an

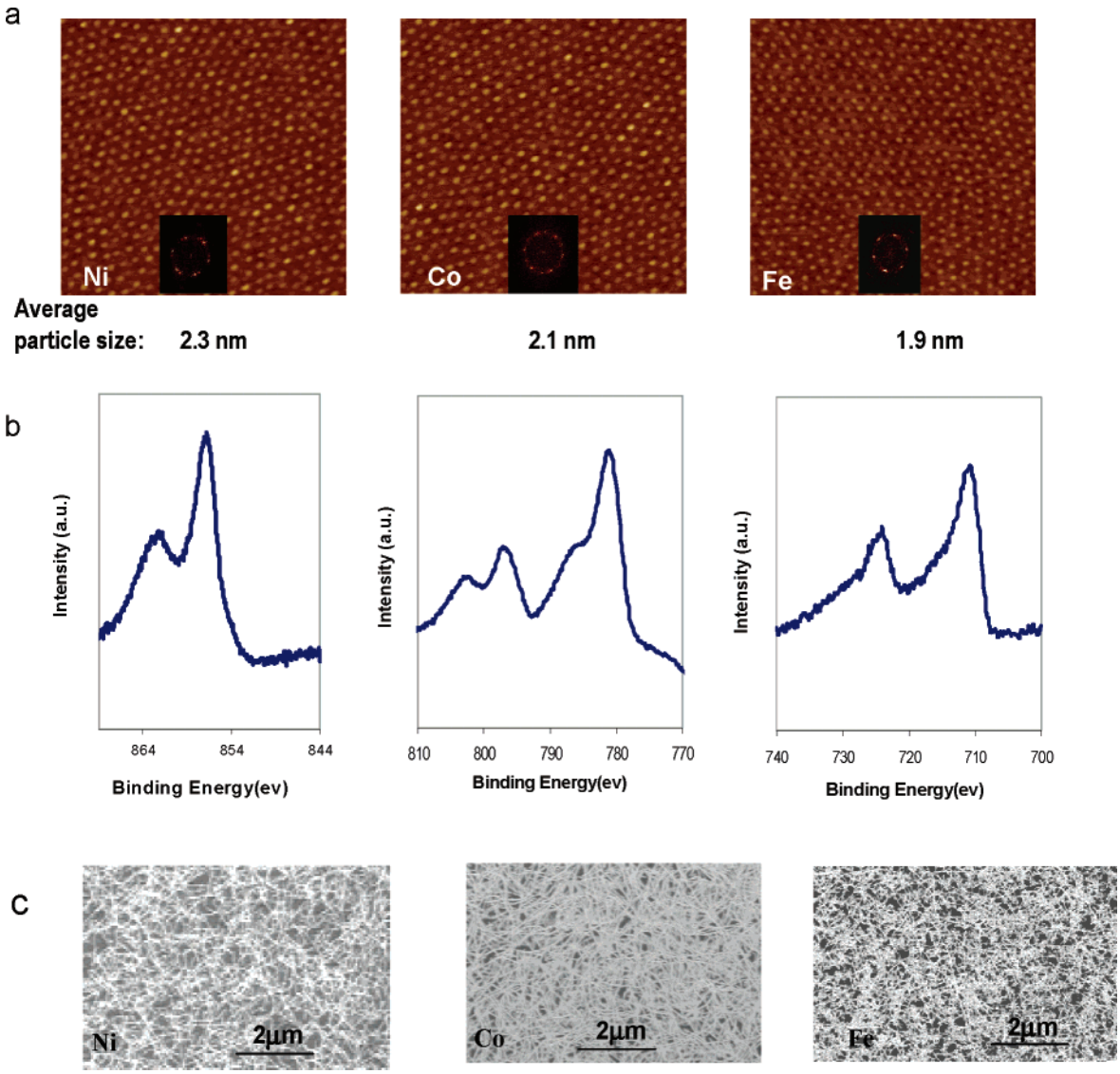


**Figure 4.** (a) AFM height images of metal nanoparticles (height scale, 10 nm; scan size, 1 $\mu$m × 1 $\mu$m). (b) Corresponding XPS spectra. (c) SEM micrographs of CNT growth results.

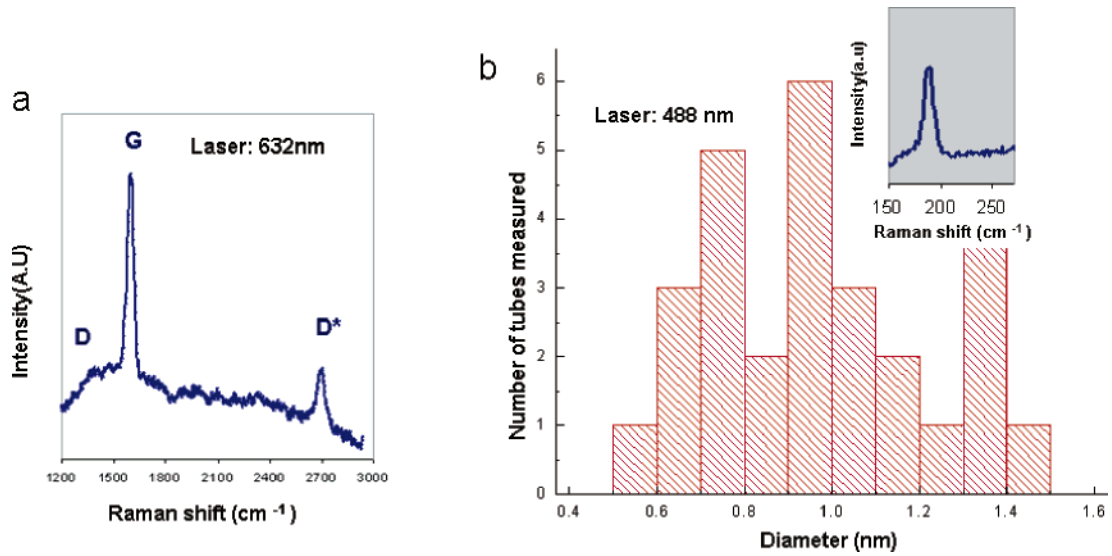


**Figure 5.** (a) Raman spectrum of CNTs produced from a cobalt catalyst. (b) Summary of AFM analysis and a representative Raman spectrum at RBM (inserted).

exposure wavelength of 365 nmand subsequently developed in a metal ion free aqueous base developer, 1:1 $H_2O$:OPD262. A slight overdevelop will etch the LOL underlayer under the exposed resist area. Acetone was used to remove the exposed

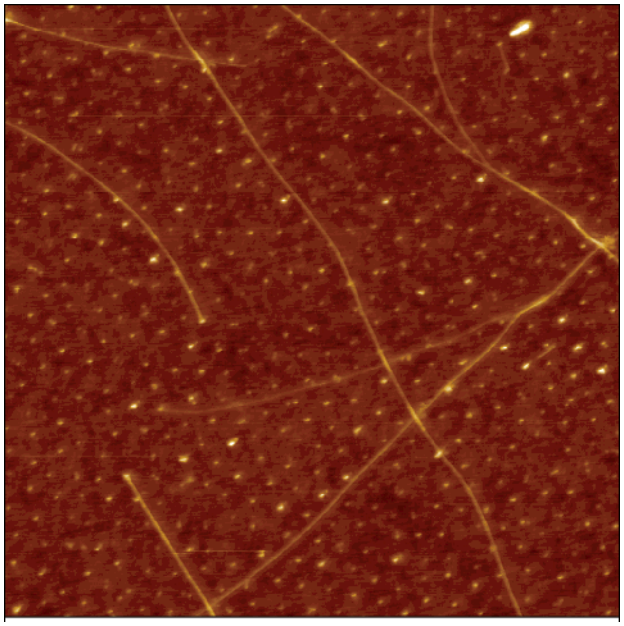

**Figure 6.** AFM image of CNTs and cobalt catalyst nanoparticles after growth (height scale, 5 nm; scan size, 1 $\mu$m × 1 $\mu$m).

OCG 825 film and leave the patterned 100 nm thick LOL1000 underlayer behind. The cobalt-containing polymer micelle solution was then deposited by spin-coating. After lifting off the LOL1000 underlayer material using the undiluted metal ion free aqueous base developer, donut-shaped cobalt micelle film patterns were then formed. The same UV-ozone process was used to remove all the organics, and the CNT growth condition was identical to that described above for full-film CNT growth.

## Results and Discussion

Figure 1 is a schematic drawing illustrating the use of block copolymer micelles to synthesize catalytically active nanoparticles for CNT growth. In this approach, polystyrene-*b*-poly(4-vinyl pyridine) forms micelles in toluene where PS, a nonpolar block, forms the corona while P4VP, a polar block, forms the core. Metal precursors are then introduced and localized in the core by selectively attaching onto the pyridine functional groups through coordination bonds. Metal-bearing micelles are subsequently deposited on to a surface by spin-coating. Subsequent UV-ozonation removes all of the organics and converts the nonvolatile metal species into metal oxide nanoparticles.

The prerequisite of using block copolymer micelles as nanoreactors to produce metallic nanoparticles is the formation of metal-containing micelles. It is known that transition metals such as iron, cobalt, and nickel have energetically accessible d orbitals. These partially filled outer electronic orbitals provide a number of reaction pathways. To satisfy the 18 electron or inert gas rule, electron-rich ligands such as nitrogen or oxygen readily complex with the empty d orbitals of transition metals. Figure 2 is a set of FTIR spectra of P4VP with and without metals. The nickel(II) modified P4VP exhibits a noticeable decrease in intensity of the C═N stretching band at 1557 and 1415 $cm^{-1}$ and the appearance of new bands at 1616 $cm^{-1}$ and 1425 $cm^{-1}$, which are characteristic of pyridine complexes with metals.[13,14] This indicates that nickel(II) has complexed well with the pyridine unit. The addition of iron(II) induces the smallest change in the IR spectrum with the inception of the new band at 1616 $cm^{-1}$ while the cobalt(II) sample shows a more intense peak at 1616 $cm^{-1}$. This result is consistent with the fact that the complexation stability with pyridine increases in the order of iron(II) < cobalt(II) < nickel(II).[15−17] The increase in stability constant as one moves across the transition metal series agrees with the Irving−Williams sequence.[18]

Due to high incompatibility of PS with PVP segments ($\chi \sim 0.1$),[19,20] spherical micelles with PS coronas and PVP cores have been formed in toluene. With the deposition of PS-P4VP solution micelles onto a 5000 Å thermally grown silicon oxide surface, surface micelles have thus been produced as demonstrated by the 3D AFM height image in Figure 3. The 2D Fourier transform analysis indicates that the distance between micelles is 34 nm, which is much greater than the 20 nm theoretical calculation of the spherical morphology periodicity. After the micelle formation in toluene, hydrated iron(II), cobalt(II), and nickel(II) chloride salts were then stirred into the polymer micelle solutions to selectively bind onto the pyridine units. The metal-bearing micelle solutions were then spin-coated onto 5000 Å silicon thermal oxide surfaces. UV-ozonation removed all the organic components, and the nonvolatile metal nanoparticles were then formed.

Figure 4a is a set of representative AFM height images of resultant nanoparticles and their associated 2D Fourier transform spectra. The average particle height produced from hydrated iron(II), cobalt(II), and nickel(II) chloride salts are 2.3, 2.1, and 1.9 nm, respectively, with a standard deviation around 0.2 nm. The 2D Fourier analysis indicates that nanoparticles are arranged in a hexagonal lattice and the separation between nanoparticles is around 32 nm. X-ray photoelectron (XPS) analysis shown in Figure 4b confirms that the nanoparticles are indeed iron, cobalt, and nickel in their oxidized forms. The peak corresponding to $Fe2p_{3/2}$ appears at 711 eV indicating that iron is in the form of iron oxide. The $Co2p_{3/2}$ peak appears at 780.2 eV and Ni $2p_{3/2}$ peak shows at 856.4 eV, consistent with the binding energy of cobalt and nickel at their highest oxidation states.[21] These results also imply that bimetallic and trimetallic catalytically active nanoparticles can be formed by complexation of more than one metal species with pyridine groups. Detailed experimental results will be published later.

Figure 4c displays typical scanning electron microscope (SEM) images of CNTs generated from these catalyst nanoparticles. As can be seen, uniformly distributed CNT mats have been synthesized. Because of the excellent processability of these polymeric systems, metallic nanoparticles have been uniformly distributed across a wafer with precise control of periodicity, resulting in evenly dispersed CNTs.

A typical Raman spectrum of CNTs produced using the cobalt nanoparticles is displayed in Figure 5a. The D band at 1380 $cm^{-1}$ is the second-order defect-induced Raman mode involving a one-phonon elastic scattering process. Thus the intensity of this peak is directly correlated with the level of defects or the number of dangling bonds in the $sp^2$ arrangement of graphene. The G band centered at 1590 $cm^{-1}$ is the first-order Raman process attributed to an in-plane oscillation of carbon atoms in the $sp^2$ graphene sheet.[22,23] The narrow width and high intensity of the G band and the absence of the D band indicate that the quality of CNTs is exceptionally high with an undetectable amount of amorphous carbon and dangling bonds. Mechanical radial oscillation of CNTs at the lower frequency region is unique to carbon nanotubes with one or few walls. Since the frequency of the radial breathing mode (RBM) is inversely proportional to CNT diameter, the diameters of CNTs can be estimated from the RBM frequencies. The tube diameters are obtained using the relationship $d$ (nm) = 233 $cm^{-1}/\omega_{RBS}$.[22,23] A slight shift to lower frequency due to overlapping of tubes was ignored.[24] The tube diameters based on Raman spectro-

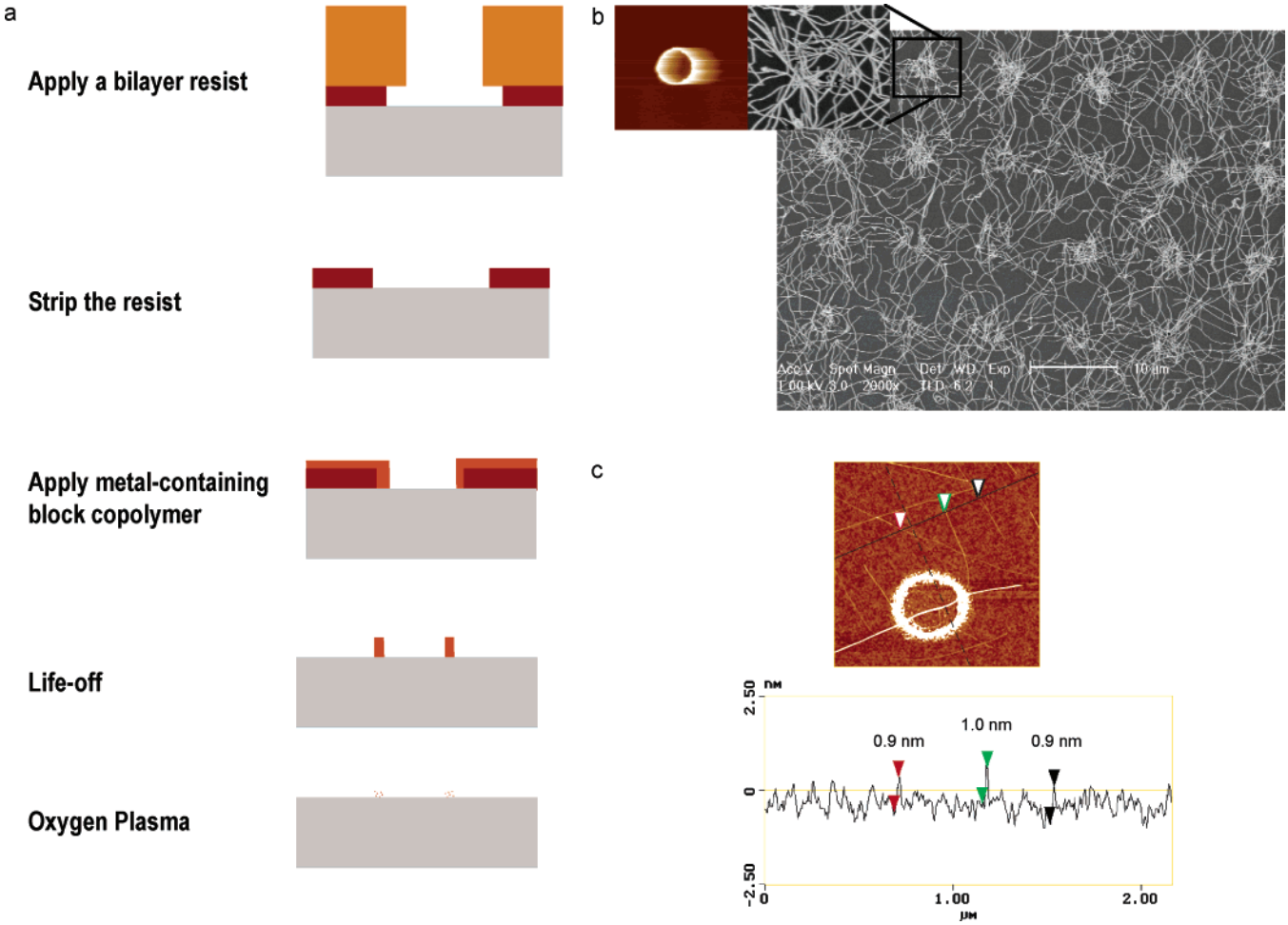


**Figure 7.** Schematic drawing of process flow for formation of a donut-shaped catalyst nanoparticle pattern. (b) A low magnification SEM micrograph of lithographically controlled growth of CNTs using patterned polymeric film of cobalt-containing micelles. AFM height image (height scale, 100 nm; scan size, 2.5 $\mu$m $\times$ 2.5 $\mu$m) of a donut-shaped pattern of the micelle film and the corresponding SEM micrograph of CNTs (inserted). (c) A representative AFM height image of as-synthesized CNTs.

scopic analysis at the RBM ranged from 0.5 to 1.5 nm, which agrees with the AFM height measurements. A characteristic Raman spectrum at the CNT radial breathing region and the summary of AFM height estimation of CNT diameters are displayed in Figure 5b. The average diameter of CNTs is 1.0 nm, slightly smaller than the size of cobalt nanoparticles, which is due to the particle shrinkage from the reduction of cobalt oxide to cobalt, solidification at elevated temperature, and sublimation of cobalt atoms before growth. The reasonably narrow CNT diameter distribution suggests that uniformly sized catalyst nanoparticles have promoted the controllable growth of CNTs. More importantly, AFM inspection on all the post grown samples indicates that the catalyst nanoparticles have not agglomerated during the growth. Figure 6 is a low yield CNT sample clearly indicating the nanoparticles have not aggregated at the high growth temperature.

Metal-containing diblock copolymers are fully compatible with conventional photoresist processes. Using a lift-off process as depicted in Figure 7a, donut-shaped catalyst patterns can be generated and selective growth of CNTs at predefined locations over a large area has been achieved. The formation of a donut-shaped pattern is the result of the preferential interaction between the polymide-based LOL1000 material and metal-bearing polymer micelle solution. Figure 7b is the AFM height image of donut-shaped polymeric patterns comprised of cobalt-bearing micelles and the corresponding SEM images of patterned growth of CNTs at low and high magnifications. Figure 7c is a representative AFM height image of CNTs produced from a donut-shaped catalyst pattern. In general, the diameters of CNTs are around 1.0 nm.

## Conclusion

In conclusion, we have demonstrated that the block copolymer micelle approach has been able to produce a variety of transition metal nanoparticles such as iron, cobalt, and nickel with controlled size and spacing. These catalytically active nanoparticles have been able to produce high quality CNTs with narrow size distribution. Because of the excellent film forming ability of the block copolymer, evenly spaced catalyst nanoparticles have been generated across a surface, resulting in uniformly distributed CNT mats. The polymer micelle approach is fully compatible with conventional resist processes. Spatially selective growth of CNTs has been realized by lithographically patterning catalyst-bearing micelle films. More importantly, these nanoparticles do not coalesce at the high growth temperature. All of the attributes provided by this method have enabled controllable synthesis of CNTs.

**Acknowledgment.** We are grateful to Rolf Jaeger, Grant Girolami, Danielle Chamberlin, Victorey Tumangan, and Mark Hueschen for support and useful discussions. The Raman spectroscopy of radial breathing modes was performed at Evans Analytical Group. J. Lu thanks Prof. Melanie Sanford at the University of Michigan for very useful discussions.

## References and Notes

(1) Fan, S. S.; Chapline, M. G.; Franklin, N. R.; Tombler, T. W.; Cassell, A. M.; Dai, H. J. *Science* **1999**, *283*, 512.

(2) Tans, S. J.; Dekker, C. *Nature* **2000**, *404*, 834. McEuen, P. L.; Fuhrer, M. S.; Park, H. K. *IEEE Trans. Nanotechnol.* **2002**, *1*, 78.

(3) Hafner, J. H.; Cheung, C. L.; Woolley, A. T.; Lieber, C. M. *Progress in Biophys. Mol. Biol.* **2001**, *77*, 73.

(4) Dai, H. J.; Hafner, J. H.; Rinzler, A. G.; Colbert, D. T.; Smalley, R. E. *Nature* **1996**, *384*, 147.

(5) Kong, J.; Franklin, N. R.; Zhou, C.; Chapline, M. G.; Peng, S., Cho, K. J.; Dai, H. J. *Science* **2000**, *287*, 622. Snow, E. S.; Novak, J. P.; Lay, M. D.; Houser, E. H.; Perkins, F. K.; Campbell, P. M. *J. Vac. Sci. Technol* **2004**, *22* (4), 1990.

(6) Kong, J.; Soh, H. T.; Cassell, A. M.; Quate, C. F.; Dai, H. J. *Nature* **1998**, *395*, 878.

(7) Javey, A.; Dai, H. J. *J. Am. Chem. Soc* **2005**, *127*, 11942.

(8) Park, M.; Harrison, C.; Chaikin, P. M.; Register, R. A.; Adamson, R. M. *Science* **1997**, *276*, 1401.

(9) Lopes, W. A.; Jaeger, H. M. *Nature* **2001**, *414*, 735.

(10) Thurn-Albercht, T.; Kastle, G. A.; Emley, N.; Shiauchi, T.; Krusin-Elbaum, L.; Guarini, K.; Black, C. T.; Tuominen, M. T. *Science* **2000**, *290*, 2126.

(11) Glass, R.; Möller, M.; Spatz, J. P. *Nanotechnology* **2003**, *14*, 1153.

(12) Fu, Q.; Huang, S. M.; Liu, J. *J. Phys. Chem. B* **2004**, *108*, 6124.

(13) Liu, M.; Yan, X.; Liu, H.; Yu, W. *React. Funct. Polym.* **2003**, *44*, 55.

(14) Bekturov, E. A. Kudaibergenov, S. E.; Kanapyanova, G. S.; Saltbaeva, S. S.; Skushnikova, A. I.; Pavlova, A. L.; Domnina, E. S. *Polym. J.* **1991**, *23* (4), 339.

(15) Kurihara M.; Kawashima, T.; Ozutsumi, K. *J. Chem. Sci.* **2000**, *55* (3−4), 277.

(16) *Stability constants of metal-ion complexes*, 2nd ed.; imprint; Pergamon Press: Oxford, New York, 1979−1982; Suppl. 2.

(17) Kapinos, L. E.; Sogel, H. *Inorg. Chim. Acta* **2000**, 131.

(18) Irving, H.; Williams, R. J. P. *Nature* **1948**, *162*, 746.

(19) Schulz, M. F.; Khandpur, A. K.; Bates, F. S. *Macromolecules* **1996**, *29*, 2857.

(20) Föster, S.; Zisenis, M.; Wenz, E.; Antonietti, M. *J. Chem. Phys.* **1996**, *104* (24), 9956.

(21) Moulder, J. F.; Stickle, W. F.; Sobol, P. E.; Bomben, K. D. *Handbook of X-ray Photospectroscopy*; Physical Electronics Inc.; 1995.

(22) Dresselhaus G.; Dresselhaus, M. S. In *Science and Applications of Nanotubes*; Tománek, D., Enbody, R. J., Eds.; Kluwer Academic: New York, 2000, p 275.

(23) Dresselhaus, M. S.; Eklund, P. C. *Adv. Phys.* **2000**, *49*, 705. Rao, A. M.; Chen, J.; Richter, E.; Schlecht, U.; Eklund, P. C.; Haddon, R. C.; Venkateswaran, U. D.; Kwon, Y. K.; Tomanek, D. *Phys. Rev. Lett.* **2001**, *86*, 3895.

(24) Rao, A. M.; Chen, J.; Richter, E.; Schlecht, U.; Eklund, P. C.; Haddon, R. C.; Venkateswaran, U. D.; Kwon, Y. K.; Tomanek, D. *Phys. Rev. Lett.* **2001**, *86*, 3895.